

3-D Multiple-level simulation of free surface flows

Simulation 3D d'écoulements multi-couches à surface libre

MARCELO REGGIO, *Professor, Department of Mechanical Engineering, École Polytechnique de Montréal, C.P. 6079, succursale Centre-ville, Montréal (Québec) H3C 3A7, Canada,*

ANDRÉ HESS, *Research Assistant, CERCA, 5160 Boulevard Décarie, bureau 400, Montréal (Québec) H3X 2H9, Canada*

ADRIAN ILINCA, *Professor, Département de mathématiques, informatique et génie, Université du Québec à Rimouski, 300 allée des Ursulines, Rimouski (Québec) G5L 3A1, Canada*

e-mail: marcello@meca.polymtl.ca, andreh@cerca.umontreal.ca, ruiliadr@uqar.quebec.ca

ABSTRACT

A 3-D multiple-layer model to describe and compute free surface flows has been applied to rivers and seashore parts. Vertical convective fluxes and shear stress at the interface are kept in the x - y momentum equation. The hydrostatic pressure of the top layer, is taken into account. The flow is calculated via a finite volume numerical scheme. The solver is based on Roe's Flux Difference-Splitting (FDS) method. The spatial discretization uses triangular elements as the basic control-volume cells. Data obtained from references, analytical solutions and real configurations have been used to evaluate the performance of the proposed method. The numerical scheme has been shown to be capable of predicting the behavior of Ekman's classical surface layer or of a simple tide wave fixed on an open boundary of a rectangular domain, for example. The evolution of a tidal constituent on the St. Lawrence estuary is also presented.

RÉSUMÉ

Un modèle multi-couches permettant la modélisation des écoulements tridimensionnels a été appliqué au calcul des écoulements fluides à surface libre tels que ceux rencontrés dans les fleuves et rivières ainsi que ceux qui se produisent sur des portions de côtes océaniques. La formulation tient compte des flux convectifs verticaux et des contraintes de cisaillement dans les équations de mouvement écrites dans le plan horizontal. On considère la pression hydrostatique pour la couche supérieure. L'écoulement est résolu numériquement par la méthode des volumes finis utilisant un schéma de Roe pour la décomposition des flux. L'élément de base de la discrétisation est le triangle. La performance de la méthode a été évaluée en résolvant des cas possédant une solution analytique et en comparant à d'autres résultats expérimentaux. Le schéma a été appliqué pour prédire adéquatement le comportement de la couche classique de Ekman et pour un domaine rectangulaire ayant une frontière ouverte. L'évolution d'un modèle de marée dans le fleuve St. Laurent est aussi présentée.

1 Introduction

Incompressible hydrodynamic flow of a nearly horizontal nature is characterized by negligible vertical acceleration when compared with gravitational acceleration. Under these circumstances, the three-dimensional Navier-Stokes equations simplify to the two momentum equations in the x - y plane, plus the divergence-free constraint representing the continuity equation. Integrating these equations over the depth, from the bottom to the free surface, and considering the velocity to be composed of a mean value and a fluctuating part leads to the well-known 2-D shallow water equations (SWE) model. Different numerical studies using finite differences and finite elements have been carried out for such hydrodynamic modeling such as in references [1], [2], [3], [4], [5] among others. An extension of a particular finite-volume scheme [6] to solve multiple coupled horizontal flows is the object of this study. Specifically, the methodology introduced by Kawahara [7], which has been applied to the calculation of tidal currents in Tokyo Bay, will be adopted. According to this approach, the multi-level system requires the treatment of several layers sharing friction terms and vertical convective fluxes. The computational method used in this study is based on the flux difference-splitting solver introduced by Roe [9], which must be judiciously applied in treating the bathymetry, i.e. the top and the

bottom friction terms. The fundamental validations for the 2-D SWE are presented first. Then, a numerical test consisting of a steady wind-induced flow in a rectangular channel is carried out. Finally, a computation regarding the St. Lawrence estuary is performed. This problem includes wind shears, a periodic tidal condition on the ocean boundary and Coriolis forces.

2 Governing equations

The Navier-Stokes equations for a constant density incompressible flow can be written as:

$$\nabla \cdot v = 0$$

$$\frac{Dv}{Dt} = -\frac{1}{\rho} \nabla P + g - 2\omega \times v + f_r$$

where ρ denotes the density, v the velocity vector, P the hydrostatic pressure, ω the Coriolis vector, g the gravitational acceleration, f_r the friction forces and $\frac{D}{Dt}$ the substantial derivative. With the assumption of negligible relative vertical convective-diffusive terms and non appreciable relative vertical acceleration when compared with gravitational acceleration, the flow behaves in nearly horizontal fashion. In the Cartesian x - y - z reference frame, the vertical momentum equation can be written as:

Revision received June 7, 2000. Open for discussion till December 31, 2002.

$$g = -\frac{1}{\rho} \frac{\partial P}{\partial z}$$

This hydrostatic pressure distribution is at the core of the shallow water concept and can be, to some extent, related to the classical 2-D boundary layer theory in which simplifications lead to, among others, the condition: $\frac{\partial P}{\partial y} = 0$.

The resulting set of equations constitutes the *3-D shallow water equations*. Integrating these equations over a *single layer* along the vertical direction using the Leibniz rule and considering that the velocity vector, v , is made up of the sum of a mean value, \bar{v} , and a residual part, v' , it is possible to obtain the classical set of two-dimensional *2-D depth-averaged SWE equations* [10].

By contrast, when *multiple layers* are taken into account [7], the integration process leads to a new set of equations which closely resembles the *SWE*, but which includes interfacial friction terms and a convective vertical term. In one sense, these equations can be seen as two-dimensional because the integration process can be performed for each layer separately. Nevertheless, by its very nature the multiple-layer approach implies various layers in the vertical direction interacting through the common interface friction and vertical velocity. Thus, they are a step closer to the three-dimensional nature of the flow without completely representing it. Figure 1 displays this multiple layer concept. For a given k^{th} layer, integration of the x -momentum with the continuity equation built-in leads to the following form:

$$\begin{aligned} & \frac{\partial uh}{\partial t} + \frac{\partial \left(uuh + \frac{1}{2} gh^2 \right)}{\partial x} + \frac{\partial uvh}{\partial y} + \\ & \int_{z_B^{(k)}}^{z_T^{(k)}} \left(\frac{\partial(uw)}{\partial z} \right) dz = -gh \frac{\partial Z}{\partial x} \\ & + f_c \bar{v}^{(k)} h^{(k)} + \frac{1}{\rho} \int_{z_B^{(k)}}^{z_T^{(k)}} \left(\frac{\partial \tau_{xx}}{\partial x} + \frac{\partial \tau_{xy}}{\partial y} \right) dz + \frac{1}{\rho} [\tau_{xT}^{(k)} - \tau_{xB}^{(k)}] \end{aligned}$$

Note that the overline used to indicate a mean value has been dropped for simplicity in this vertically averaged equation. A sim-

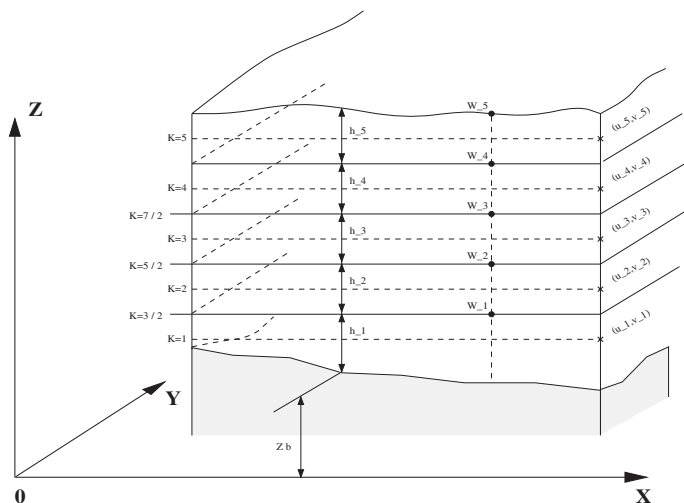


Fig. 1 Multiple-layer configuration

ilar form of the expression holds for the y -momentum equation. The integral counterpart of the 3-D shallow water equations will now be presented.

2.1 Finite Volume Formulation

The multi-layer SWE can be written in conservative or nonconservative form. According to the finite volume spatial discretization that is applied, the conservative formulation is used. The system can now be written for a typical k^{th} layer in compact form as:

$$\int_v \left(\frac{\partial f}{\partial t} + \frac{\partial G}{\partial x} + \frac{\partial H}{\partial y} \right) dV = - \int_v (R - \nabla \cdot D + B + S) dV \quad (1)$$

where:

$$f = \begin{bmatrix} h \\ uh \\ vh \end{bmatrix}, \quad G = \begin{bmatrix} uh \\ uuh + \frac{1}{2} gh^2 \\ uvh \end{bmatrix}, \quad H = \begin{bmatrix} vh \\ uvh \\ vvh + \frac{1}{2} gh^2 \end{bmatrix}$$

$$R = \begin{bmatrix} 0 \\ gh \cdot \frac{\partial z}{\partial x} \\ gh \cdot \frac{\partial z}{\partial y} \end{bmatrix}, \quad D = \begin{bmatrix} 0 \\ v [\nabla U + (\nabla U)^T] \end{bmatrix}$$

with

$$U = [uh, \quad v h]^T, \quad B = \begin{bmatrix} 0 \\ C_f uh \\ C_f v h \end{bmatrix}, \quad S = \begin{bmatrix} 0 \\ S_x \\ S_y \end{bmatrix}$$

and

$$S_x = \int_{z_B}^{z_T} \left(\frac{\partial(uw)}{\partial z} \right) dz - f_c \quad v h - [\tau_{xT} - \tau_{xB}]$$

$$S_y = \int_{z_B}^{z_T} \left(\frac{\partial(vw)}{\partial z} \right) dz + f_c \quad uh - [\tau_{yT} - \tau_{yB}]$$

f_c in the previous expression is the Coriolis parameter. The vertical turbulent shear stresses in the above expressions:

$\tau_{xT}^{(k)}$, $\tau_{yT}^{(k)}$, $\tau_{xB}^{(k)}$, $\tau_{yB}^{(k)}$ are given by [7], [11]:

$$\tau_{xT}^{(k)} = \frac{\partial}{\partial x} \left(A_v \frac{\partial u}{\partial z} \right); \quad \tau_{yT}^{(k)} = \frac{\partial}{\partial z} \left(A_v \frac{\partial v}{\partial z} \right)$$

where A_v is a parameter analogous to the kinematic viscosity defined as:

$$A_v = f_{ric} \left| \frac{\partial u}{\partial z} \right|$$

Similarly, the term $v[\nabla U + (\nabla U)^T]$ embodies the horizontal turbulent shear stresses. These come from the terms in the horizontal x - y directions i.e.:

$$\frac{1}{\rho} \int_{z_b^{(k)}}^{z_t^{(k)}} \left(\frac{\partial \tau_{xx}}{\partial x} + \frac{\partial \tau_{xy}}{\partial y} \right) dz \quad \text{and} \quad \frac{1}{\rho} \int_{z_b^{(k)}}^{z_t^{(k)}} \left(\frac{\partial \tau_{yx}}{\partial x} + \frac{\partial \tau_{yy}}{\partial y} \right) dz$$

In the above expression, v is normally taken as a constant. In the current study, the value of $v = 0.01 \text{ m}^2 \text{ s}^{-1}$ has been used for the validation test.

For the deepest layer and the surface layer, the vertical turbulent stresses are given by semi-empirical formulas. These are, respectively:

surface layer:

$$\frac{\tau_{xT}^{(k)}}{\rho_a} = C_D W_x (W_x^2 + W_y^2)^{1/2}; \quad \frac{\tau_{yT}^{(k)}}{\rho_a} = C_D W_y (W_x^2 + W_y^2)^{1/2}$$

with $C_D = 1.5 \times 10^{-4}$ to 2.5×10^{-6} (drag coefficient)

bottom layer:

$$\frac{\tau_{xB}^{(k)}}{\rho} = C_f uh; \quad \frac{\tau_{yB}^{(k)}}{\rho} = C_f vh$$

with $C_f = \frac{gN^2(u^2 + v^2)^{1/2}}{h^{4/3}} \text{ [s}^{-1}\text{]}$ and

$N =$ Manning coefficient

For each layer of the governing equations, the vertical velocity w is obtained from the continuity equation taking into account the contribution of the time elevation derivatives of the layers underneath. In particular, $w^{(k)}$ is given by:

$$\frac{\partial h}{\partial t} = w^{(k)} = - \sum_{l=1}^k \left(\frac{\partial uh^{(l)}}{\partial x} + \frac{\partial vh^{(l)}}{\partial y} \right) \quad (2)$$

A multi-layer formulation needs to consider the hydrostatic pressure (p_*) of the 'water column' above an internal layer. In this respect, the following term is added to the gradient of the bathymetry:

$$p_*^{(l)} = - \sum_{k=l+1}^{k_{\max}} gh^{(k)} \quad (3)$$

One also needs to be aware of the 'evolution' of the boundary conditions which depend on the layer that is being computed. In fact, different types of boundary conditions have to be considered for different layers as well, particularly at places where open boundaries turn into solid ones due to the bathymetry. This idea is illustrated in (Fig. 2).

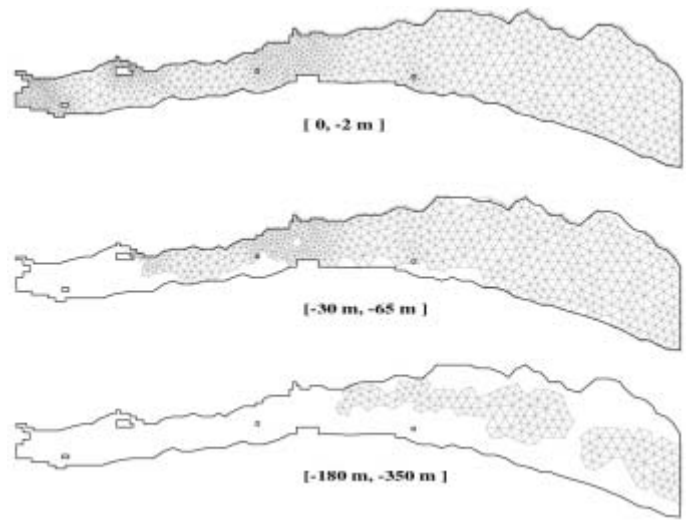


Fig. 2 Computational domain at different depths

3 Discretization

The discretization of Eq. (1) is carried out with the conservative variables f assumed to be piecewise constants over the cells. The solution is advanced from time t to time $t + \Delta t$ following an explicit method. For a control-volume cell, this yields to the local discretized equations:

$$V(f^n - f) + \Delta t \sum S(G + H - D) = -\Delta t V(R + B + S) \quad (4)$$

where V refers to the volume of the cell; quantities with and without the superscript n are evaluated at time $t + \Delta t$ and at time t respectively. The following describes how the different terms in the 3-D SW finite volume formulation will be addressed.

3.1 Roe's Solver

Roe's very popular method is well known for simulating compressible flows ([9], [12], [13]), as well as for calculating 2-D shallow-water flows in environments with a flat bed [14], is extended and used as a computing mechanism for the solution of the multiple-layer 3-D SWE. Using the standard subscripts L and R to indicate the left and right elements of a given side, the 'upwinded' flux F (with $F = G \cdot n_x + H \cdot n_y$) along a face is computed by:

$$F = \frac{1}{2}(F_L + F_R) - \frac{1}{2}P|D|P^{-1} \Delta f \quad (5)$$

where $|D| \equiv \text{diag}(|\lambda_1|, |\lambda_2|, |\lambda_3|) = \text{diag}(|u+c|, |u-c|, |u|)$ while the term $P|D|P^{-1} \Delta f = |A| \Delta f$ characterizes the amount of upwinding (left or right). The P and P^{-1} terms denote the corresponding right and left eigenvectors respectively. In order to compute the $|A|$ term, values have to be defined at the cell faces. Roe's averaging is a simple method for calculating variables along the faces of an element, the averaged variables being given

by:

$$\begin{aligned} h &= \sqrt{h_R h_L} \\ c^2 &= gh = \frac{1}{2}g(h_R + h_L) \\ u &= \frac{\sqrt{h_R} u_R + \sqrt{h_L} u_L}{\sqrt{h_R} + \sqrt{h_L}}; \text{ with } u = [u, v]^T \end{aligned} \quad (6)$$

where the subscript L indicates the cell itself such that the following jump condition is satisfied:

$$\Delta F = A \Delta f$$

From the computational point of view, it is interesting to note that the 'upwinded' flux at an interface can also be defined via the expression:

$$F = F_L + \frac{1}{2} \Delta F - \frac{1}{2} P |D| P^{-1} \Delta f \quad (7)$$

because $\Delta F = P D P^{-1} \Delta f$,

$$\Delta F = P D P^{-1} \Delta f$$

or even as:

$$F = F_L + \frac{1}{2} P (D P^{-1} \Delta f - |D| D^{-1} P^{-1} \Delta f)$$

Moreover, if the relation $\alpha = D P^{-1} \Delta f$ is used to calculate the flux we only have to consider the sign of $\sigma = |D| D^{-1}$. In fact, once the α coefficients are known, then for the geometric properties of a polygon, the summation over the element sides satisfies:

$$\sum_{i=1}^3 F_i \cdot S_i = 0 \quad (8)$$

Thus, the finite-volume balance reduces to the very convenient form:

$$\sum_{i=1}^3 F_i = \frac{1}{2} (1 - \sigma_i) \alpha_i \quad (9)$$

This equation clearly illustrates a further point that still has to be resolved before it is applied: the equation is not continuous at critical points (where $|u| = c$). In order to overcome this discontinuity, the diagonal matrix σ in Eq. (9) is modified to $\bar{\sigma} = 1, 2, 3$ as follows:

$$\begin{aligned} \bar{\sigma}_i &= 1 - \frac{|\lambda_i| - \lambda_i}{\bar{\lambda}_i} \\ \bar{\lambda}_i &= \max\{|\lambda_i|, \varepsilon\} \end{aligned} \quad (10)$$

where ε is a small constant which acts as a damping term in

Eq. (10) near the critical regimes.

3.2 Bed-Slope Upwinding

A natural discretization for the bed slope appears to be one based on a linear interpolation because bathymetry is dependent on geometry. However, if the momentum equations for the case of a zero velocity field are examined, it will be discovered that the following equation must be satisfied *within the cell*:

$$\sum S c^2 \nabla Z = 0 \quad (11)$$

Unfortunately, this is *always* the case for any bottom bed, because according to the fundamental finite volume approach, the properties are constant within the element. Therefore, to include the bed-slope effect, an attempt could be made to consider the required derivatives at the cell faces. However, these are discontinuous at the control-volume faces and if a simple averaging or smoothing were applied, the bed slope term would *no longer respect* Eq. (11). In such a case, the simulation of a flow in which ($u = 0$) will create a motion.

In order to recover the formulation of this failure, the following *approximation* is used:

$$\int_V gh \nabla Z \, dV \cong \int_V \nabla [gh(Z - Z_C)] \, dV \quad (12)$$

In this relation, Z_C represents the (constant) volume-averaged value of the bed-slope, while Z indicates a function that varies within the element. Note that the term $\int_V (Z - Z_C) \nabla (gh) \, dV$, which completes the equality, has been neglected (ref. [6]). The importance of this approximation is that Gauss' divergence theorem can now be applied to Eq. (12) and, consequently, the bathymetry term will be taken into account along the sides of the control volume rather than within it. That is:

$$\int_V \nabla [gh(Z - Z_C)] \, dV = \oint_{\partial V} gh(Z - Z_C) \, dS \quad (13)$$

This manipulation allows the bed-slope term to be approximated using upwinding in a similar manner as for the convective part. In fact, introducing a bed elevation calculated as the algebraic average of the bed elevations on two neighboring cells, by noting $Z_C = Z_L$, Eq. (11) yields:

$$\sum S n c^2 \left(\frac{Z_R + Z_L}{2} - Z_L \right) = \sum S \frac{1}{2} n c^2 \Delta Z \quad (14)$$

The term including R in Eq. (14) can therefore be expressed by:

$$\begin{aligned} V R &= \sum S \frac{1}{2} \begin{bmatrix} 0 \\ c^2 n_x \\ c^2 n_y \end{bmatrix} \Delta Z \\ &= \sum S \frac{1}{2} \xi \Delta Z \end{aligned} \quad (15)$$

Following a similar upwinding procedure to approximate the con-

vective term F , a (perhaps striking) upwinding according to the signs of the A -eigenvalues is included in this formula. In particular, Eq. (15) is modified to:

$$V R = \sum S \frac{1}{2} [\xi \Delta Z - P \sigma P^{-1} \xi \Delta Z] \quad (16)$$

with $\sigma = \text{diag}(\text{sign}(\lambda_1), \text{sign}(\lambda_2), \text{sign}(\lambda_3)) = \text{diag}(\sigma_1, \sigma_2, \sigma_3)$.

3.3 Diffusive Terms

To approximate the diffusive terms within the finite-volume framework, a working subelement is defined (see Fig. 3). This is done as follows: for each pair of triangles sharing a face, the centroid is linked to the midpoint of the two triangle sides that are not common. Accordingly, an area V_s related to a side is defined as the sum of the two closed subcells.

For these diffusive terms, the expression $v[\nabla U + (\nabla U)^T]$ appearing in Eq. [1] must be interpreted. The normal diffusive term, D , is therefore given by:

$$D = \begin{bmatrix} 0 \\ v[\nabla_n U + \nabla U] \end{bmatrix}$$

A gradient of a quantity Φ along a face is then approximated by its averaged value over V_s .

$$\begin{aligned} \nabla \Phi &= \frac{1}{V_s} \int_{V_s} \nabla \cdot (\Phi I) dV \\ &= \frac{1}{V_s} \oint_{\partial V_s} \Phi dS \end{aligned} \quad (17)$$

Under the assumption that the variables are piecewise constants, and using average values along the faces, Eq. [17] may be arranged as:

$$\nabla \Phi = \frac{S}{V_s} \Delta \Phi + \frac{1}{4V_s} \sum_{i=1}^2 [S_{R_i} (\Phi_{R_i} - \Phi_R) + S_{L_i} (\Phi_{L_i} - \Phi_L)] \quad (18)$$

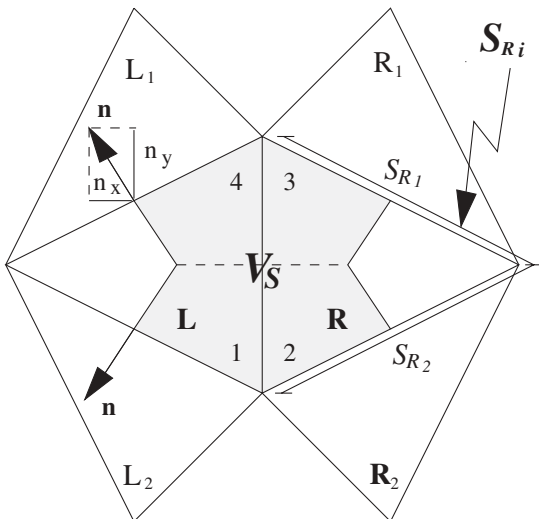


Fig. 3 Area V_s for the diffusive terms

with $\Delta \Phi = \Phi_R - \Phi_L$. Then the normal component is given by:

$$\begin{aligned} \nabla_n \Phi &= \frac{S}{V_s} \Delta \Phi + \frac{1}{4V_s} \\ &\sum_{i=1}^2 [n \cdot S_{R_i} (\Phi_{R_i} - \Phi_R) + n \cdot S_{L_i} (\Phi_{L_i} - \Phi_L)] \end{aligned} \quad (19)$$

Treating Φ as U or U , the diffusive term D is therefore evaluated using Eqs. [18] and [21].

3.4 Vertical Shear Stresses and Convection Terms

For a multiple layer formulation, the discretization of vertical convection terms that have been neglected in the 2-D SW formulation must now be considered. These vertical convective flux terms appearing in the 3-D SWE are approximated in a simple manner as follows:

$$\begin{aligned} (uw)^{(k+1/2)} &= w^{(k)} \frac{1}{2} (u^{(k+1)} + u^{(k)}); \\ (vw)^{(k+1/2)} &= w^{(k)} \frac{1}{2} (v^{(k+1)} + v^{(k)}) \end{aligned}$$

$$\begin{aligned} (uw)^{(k-1/2)} &= w^{(k)} \frac{1}{2} (u^{(k-1)} + u^{(k)}); \\ (vw)^{(k-1/2)} &= w^{(k)} \frac{1}{2} (v^{(k-1)} + v^{(k)}) \end{aligned}$$

Following the procedure described in [7], the turbulent shear stresses in expressions (1) for the bottom of a middle k^{th} layer are approximated by:

$$\frac{\tau_x^{(k)}}{\rho} = f_{\text{int}} (u^k - u^{k-1})^2; \quad \frac{\tau_y^{(k)}}{\rho} = f_{\text{int}} (v^k - v^{k-1})^2$$

A similar expression holds for the top shear stresses on a middle layer.

4 Boundary conditions

A peculiar characteristic of the current formulation is that the boundary condition treatment is performed only on the basis of the α terms. The flux F given by Eq. (7) with the right boundary defined as the boundary itself, i.e. $F = F_R$ can be written as:

$$F = F_L + \frac{1}{2} \Delta F - \frac{1}{2} P |D| P^{-1} \Delta f \quad (20)$$

Then, following an analogous methodology as with the development of Eq. (9) yields

$$(\sigma_i + 1) \alpha_i = 0, \quad (i = 1, 2, 3) \quad (21)$$

Note that the above α terms are given by $\alpha = DP_{-1} \Delta f$ instead of the

usual definition of $\alpha = P_{-1} \Delta f$. In particular:

$$\alpha = \frac{1}{2c} \begin{bmatrix} c\Delta U + U\Delta u + c^2\Delta H \\ c\Delta U - U\Delta u - c^2\Delta H \\ -2cU\Delta v \end{bmatrix} \quad (22)$$

Eq. (21) has all that is needed for the boundary condition problem because a trivial equation is obtained each time that σ_i takes the value -1 along a boundary. This tells us that a condition must be specified along such a boundary. It is a peculiar characteristic of the current formulation that allows the boundary condition treatment be implemented only on the basis of the α terms. The most common situations that arise at the boundaries are briefly discussed below.

4.1 Inflow-Outflow

For a *subcritical inflow* boundary, $-c < u < 0$ with $u = u \cdot n$. Thus, Eq. (21) with $\sigma_1 = 1$ results in the expression: $\alpha_1 = 0$, at the same time that $\sigma_2 = \sigma_3 = -1$ leads to two trivial equations which indicate that two boundary conditions must be specified.

For a *supercritical inflow* boundary, $u < -c$ and $\sigma_1 = \sigma_2 = \sigma_3 = -1$. This yields three trivial equations, and a corresponding number of conditions must be specified along boundaries of this type.

For a *subcritical outflow* boundary, $c > u > 0$, $\sigma_1 = \sigma_3 = 1$, $\sigma_2 = -1$. This type of boundary condition can be treated in the same manner as the inflow condition.

For a *supercritical outflow* boundary, the condition $u > c$ implies that $\sigma_1 = \sigma_2 = \sigma_3 = 1$, following the general relation (18), no trivial equation occurs. Therefore, no condition needs to be specified on such boundaries. This yields the well-known numerical boundary condition for which all properties are extrapolated ($f_R = f_L$). Additional details can be found in refs. [6], [8].

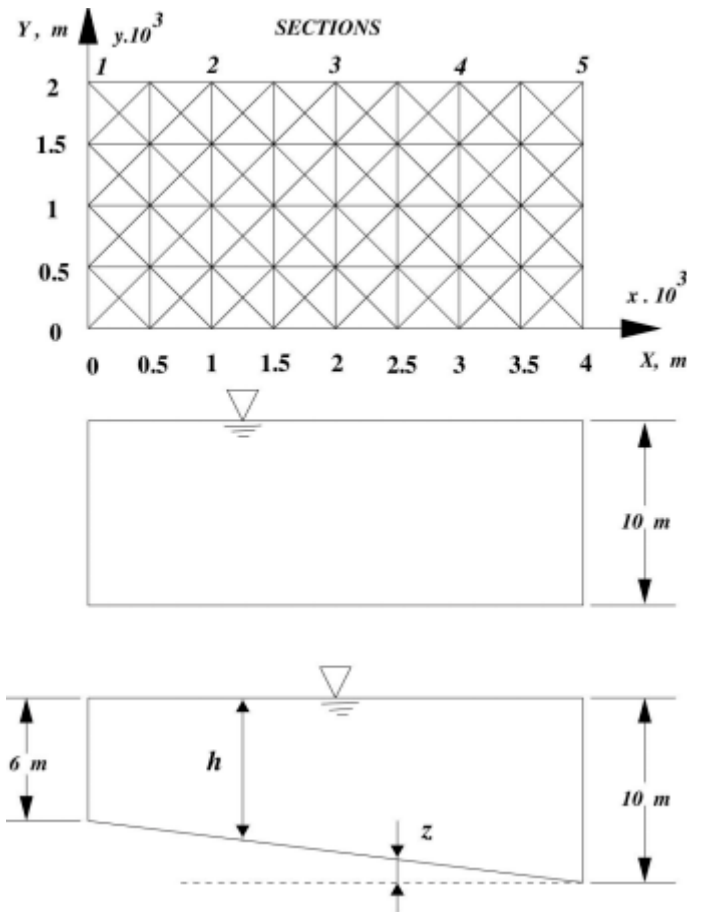


Fig. 4 Grid and 2 types of bathymetry

5 Validations and Results

5.1 Tidal Wave Propagation

This first application is the well-known study of the propagation of a linear wave in a rectangular channel [5]. This case is used to validate the capacity of the model to reproduce the vertical struc-

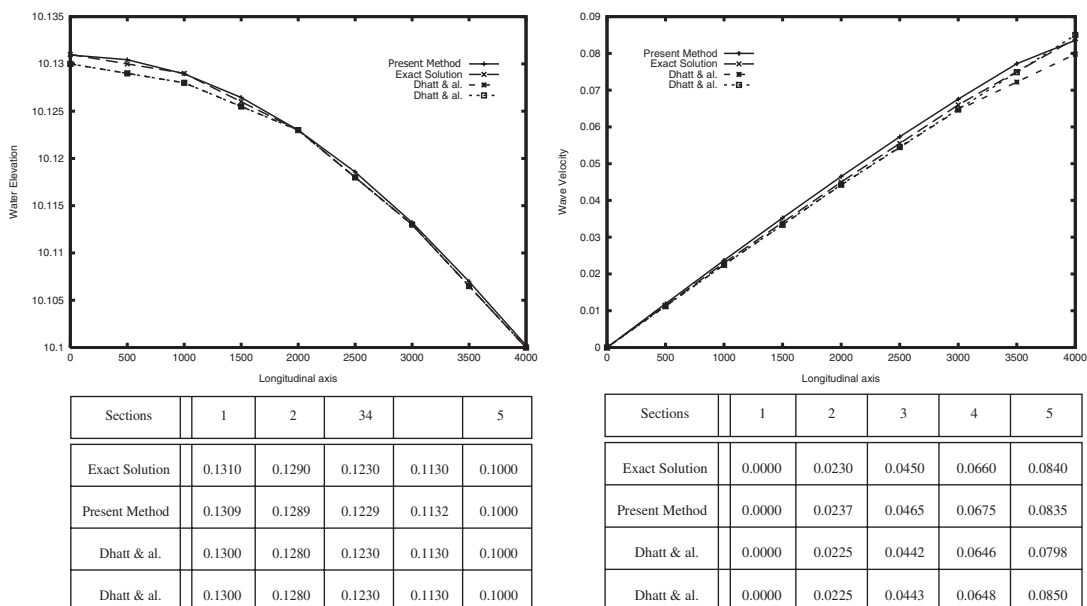
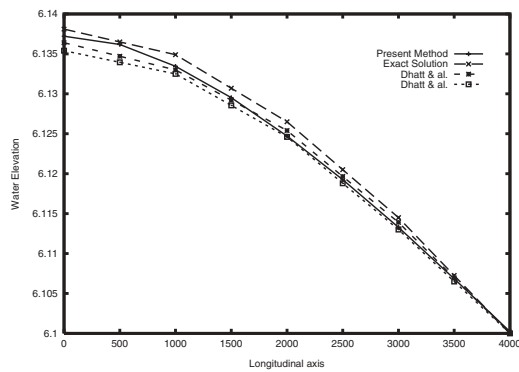
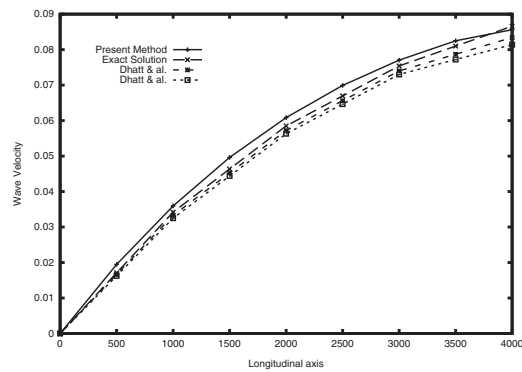


Fig. 5 Water elevation (left) and wave velocity (right) for Slope = 0



Sections	1	2	3	4	5
Exact Solution	0.1381	0.1349	0.1265	0.1145	0.1000
Present Method	0.1372	0.1334	0.1247	0.1132	0.1000
Dhatt & al.	0.1364	0.1330	0.1254	0.1139	0.1000
Dhatt & al.	0.1354	0.1325	0.1246	0.1130	0.1000



Sections	1	2	3	4	5
Exact Solution	0.0000	0.0342	0.0585	0.0754	0.0866
Present Method	0.0000	0.0359	0.0608	0.0770	0.0856
Dhatt & al.	0.0000	0.0333	0.0572	0.0740	0.0834
Dhatt & al.	0.0000	0.0325	0.0563	0.0730	0.0814

Fig. 6 Water elevation (left) and wave velocity (right) for $Slope = 10^{-3}$

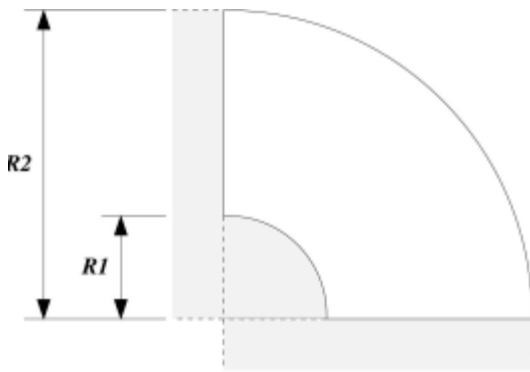


Fig. 7 Quarter-annular 'coastal domain'

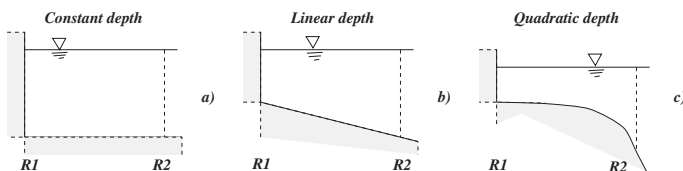


Fig. 8 Quadratically varying bathymetry

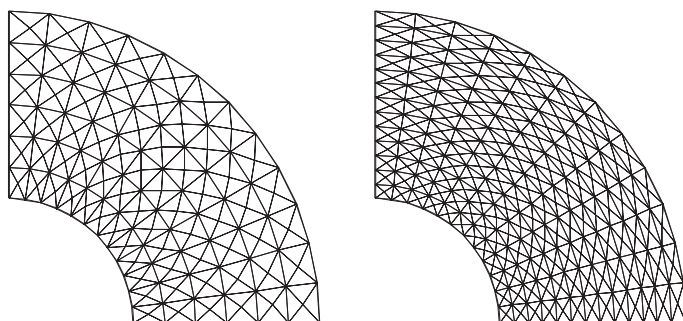


Fig. 9 Coarse and fine grids

ture of the flow. It is not a complete 3-D case, because there is no change in the lateral direction. The boundary conditions for this problem are: $u = 0$ at $x = x_0$ and $h = a \cos(\omega t)$ at $x = L$ with $a \equiv$ amplitude $= 0.1$ m, $\omega = 2\pi f$ the periodic frequency; $f = 1/T$,

and $T \equiv$ the period of one tidal component which is the so-called M_2 period $\rightarrow T = 12.42$ h. The non-slip velocity condition, $v = 0$ is imposed at the bottom of the channel. The numerical results are compared with the exact solution given by the analytical formula [15] and the finite element method proposed by Dhatt et al. [5] for two different types of elements. Our finite volume calculations agree well when compared with the exact solution, and slightly overestimate the solutions obtained in [5]. Figs. 5 and 6 illustrate these comparisons.

Another configuration of a tidal flow is given by Matsoukis [10] for a quarter-annular geometry (Fig. 7). Lynch and Gray [15] developed an analytical solution for a tidal flow with the bathymetry varying according to $H = H_0 R^n$ where H_0 is a constant, R is the radial axis and n is an integer. Different types of bathymetry are tested for comparative purposes: a) constant depth at 30 ft with ($n = 0$), b) linear depth starting from 6 m (20 ft) at $R = R_1$ to 50 ft at $R = R_2$ with ($n = 1$), and c) quadratic depth starting from 3 m (10 ft) at $R = R_1$ to 18.75 m (62.5 ft) at $R = R_2$ with ($n = 2$). The dimensional attributes for the problem are the following: $R_1 = 20 \cdot 10^4$ ft and $R_2 = 50 \cdot 10^4$ ft. Two grid sizes are used: starting at $R = R_1$, one with 7 radial interval (coarse grid) and another with 14 intervals (fine grid). The same tidal boundary condition as for the rectangular channel was fixed at $R = R_2$, i.e. $H = a \cos(\omega t)$ with an amplitude $a = 0.03$ m and a tidal period $T = 12.4$ h. The quadratic case is evaluated on a finer grid (28 intervals), resulting in a radial velocity very close to the analytical solution. This is achieved by iterating the numerical scheme for 2 or 3 cycles with a value of $N = 0.015$ for the Manning coefficient. Figs. 10 and 11 display the computed results.

5.2 Wind-induced Flow

A study of steady wind-induced flow is treated to validate the three-dimensional model. It consists of a rectangular channel with a constant depth of 10 m and a length of 1000 m. The other boundary and initial conditions for this simulation are specified as follows: a) a wind-induced velocity of $10 \text{ m} \cdot \text{s}^{-1}$ on the free sur-

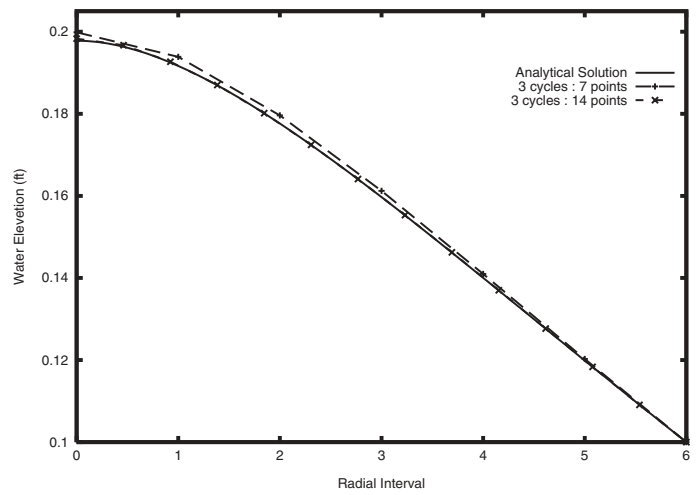
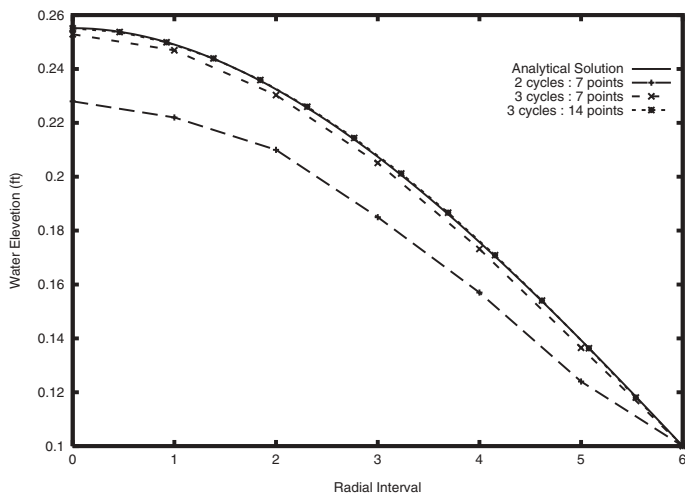


Fig. 10 Water elevation: constant depth (left) and linear depth (right)

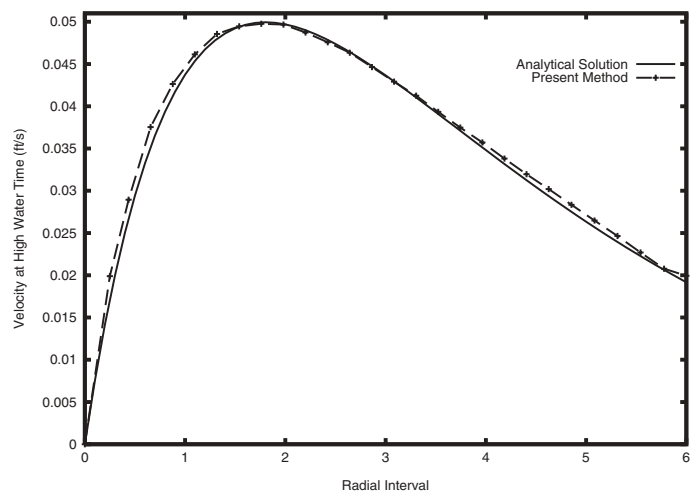
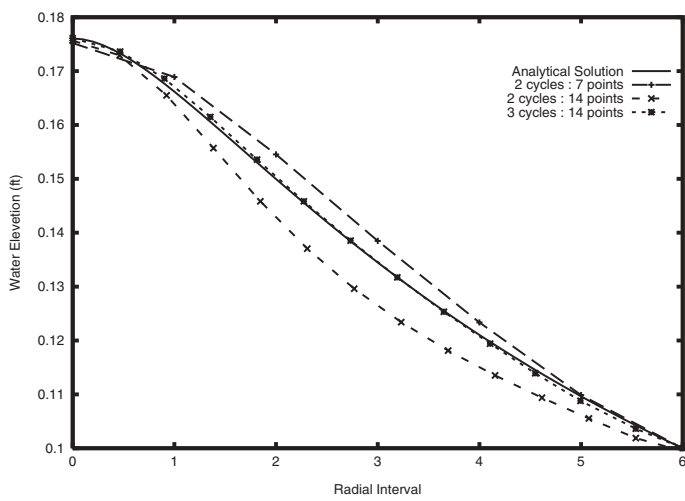


Fig. 11 Quadratic depth: water elevation (left) and wave velocity (right)

face layer, a constant water elevation at both open ends, a friction coefficient $f_{ric} = 0.002$ and a Manning coefficient $N = 0.01$. An analytical expression is given by [16] and reproduced by [7] as the following normalized expression $U = H(3H - 2)$, where $H = 1$

is the total normalized depth of the rectangular channel and U the normalized longitudinal velocity. Figs. 12 and 14 demonstrate the computational method's ability to reproduce the analytical expression.

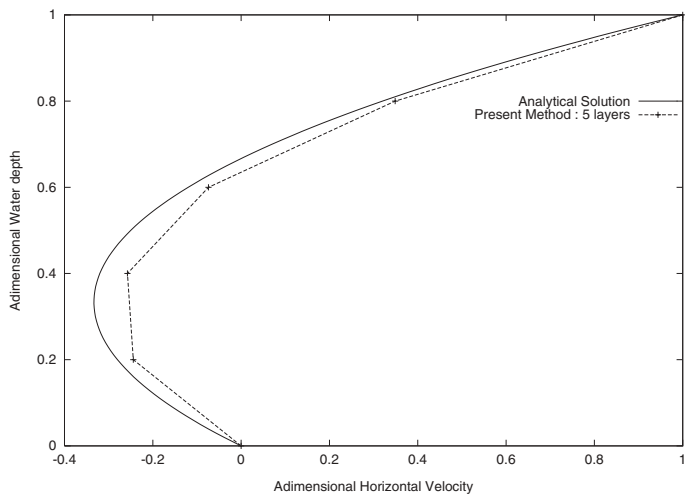


Fig. 12 Numerical and analytical profiles (5 pts)

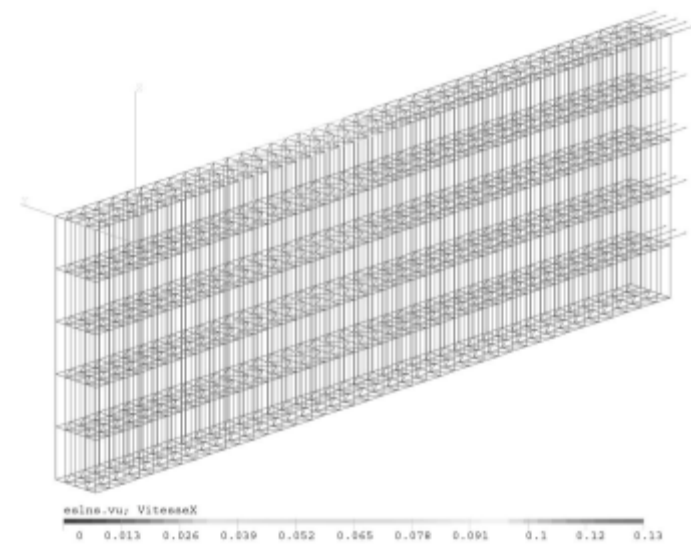


Fig. 13 Velocity field

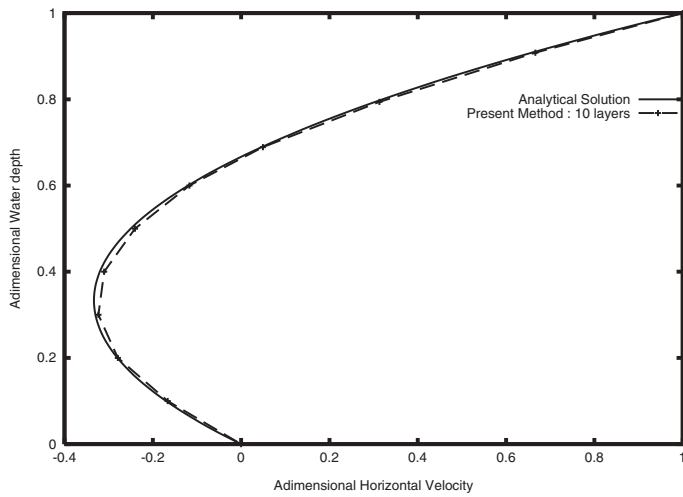


Fig. 14 Numerical and analytical profiles (10 pts)

5.3 The St. Lawrence Estuary

This complex northern river consists of a drainage basin of the so-called St. Lawrence system which encompasses an area of approximately 1 307 000 km². The basin contains the five biggest lakes in the world providing for the system's water source 4000 km inland. The hydrodynamic system modeled for this study extends from Quebec City (at the middle of Ile d'Orléans) to Pointe-des-Monts (at the widening of the river into the Gulf of St. Lawrence) 400 km seaward. The primary objective of this method is to provide an alternative to existing methods for the study of very complex interactions between stratified layers, rapidly varying bathymetry and tidal effects. At this stage, efforts have mostly been concentrated on the capability of the numerical multi-layer method to handle real-life geometries, while excluding the physics of a variable density due to salinity. In spite of this simplification at the model level, the computational method shown its ability to reproduce the residual circulation and wave propagation in the estuary. This has been attributed to the steep bathymetry in the particular region where the computation was performed. However, the current approach can not reproduce density-propelled recirculation. Even without taking into account the different densities of the vertical layers caused by salinity, the computational method has demonstrated its ability to reproduce the residual circulation and wave propagation in the estuary.

As observed by CHASSÉ [17] in his large and exhaustive work in which he combined extensive and varied simulation results mixing tidal, density and wind-driving effects, we were able to observe the same energy conservation pattern. This finite-volume method provides consistent reproductions of the main circulation, gyres and wave amplitudes moving within the estuary and, for this conservative numerical scheme, the contraction of co-amplitude and co-phase lines in narrower regions and in shallow water. Figures 17, 18, and 19 display these computed results. In the lower estuary, which is deeper and wider, tidal waves enter the estuary along the north shore with sparser co-phase lines moving progressively inside the domain. The principal parameters and specifications for this simulation are given as follows: A tidal

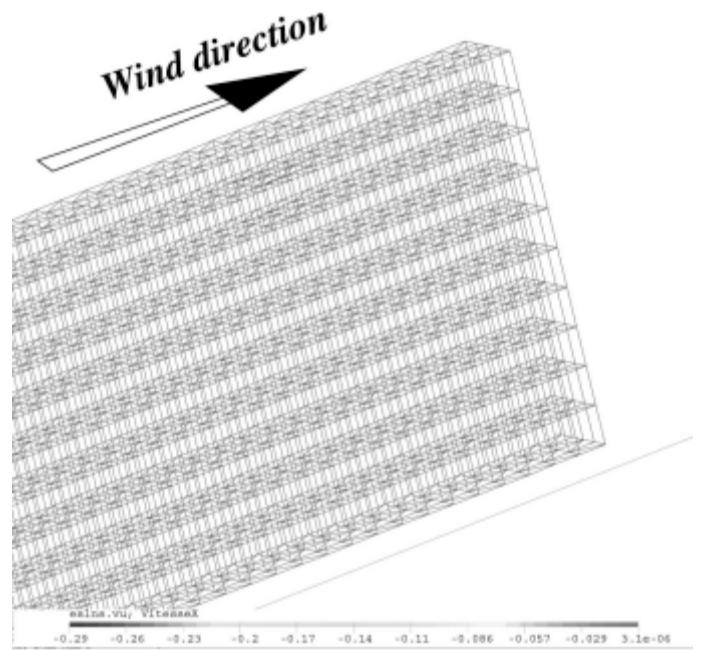


Fig. 15 Grid view

wave condition fixed on the open ocean boundary expressed as: $h = a \cos(\omega t + \phi)$ with respectively h representing the water elevation, a the amplitude of the tidal wave, $\omega = \frac{2\pi}{T}$ is the periodic frequency of a tidal constituent and ϕ the phase delay. The St. Lawrence estuary is an area influenced by the four main tidal constituents (M_2 , S_2 , K_1 , O_1). The M_2 tidal constituent in particular is examined in this study, and additional mathematical information on the specific treatment of this non-reflective boundary condition is given in refs. [6] and [8]. Also, for large domains, it is preferable to impose such a boundary specification as a function of the spatial coordinates x, y [17], while the water elevation is expressed

$$h_i(x, y, t) = \sum_{i=1}^{N_c} a_i(x, y) \cos(\omega_i t + \phi_i(x, y)).$$

Here h_i is the water elevation, a_i the amplitude, ω_i the angular frequency, ϕ_i the phase delay and N_c the number of constituents

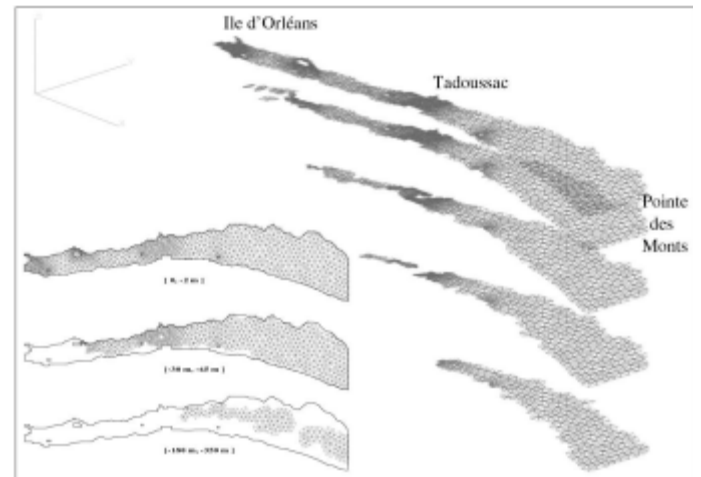


Fig. 16 Multiple-layer configuration

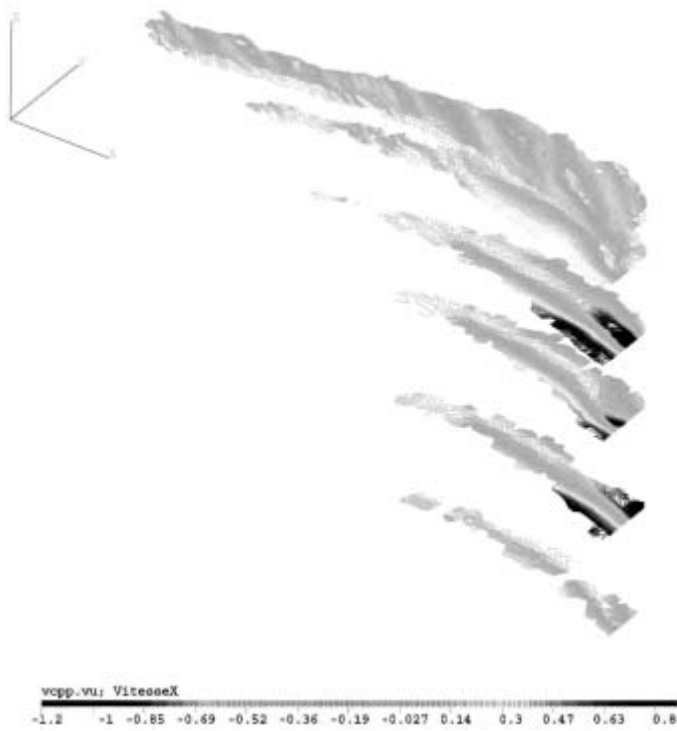


Fig. 17 Longitudinal velocity field ($\text{m}\cdot\text{s}^{-1}$)

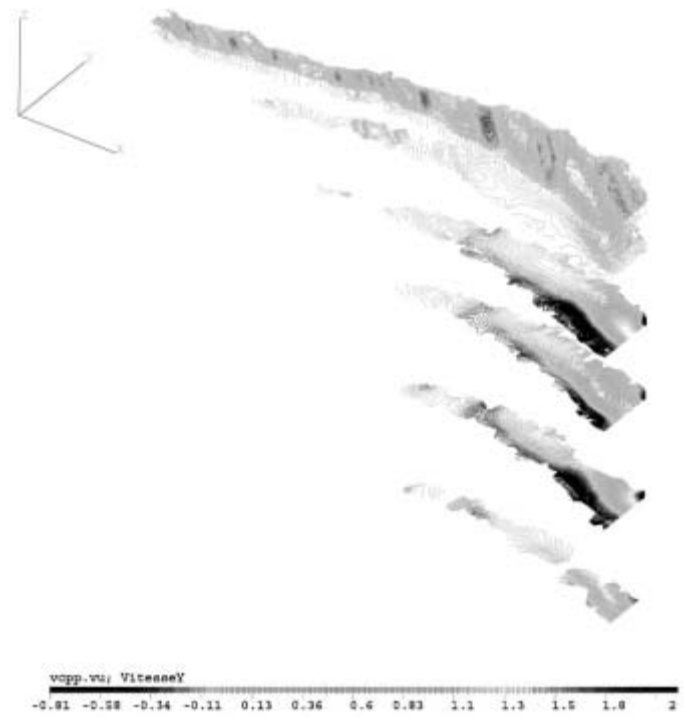


Fig. 18 Transversal velocity field ($\text{cm}\cdot\text{s}^{-1}$)

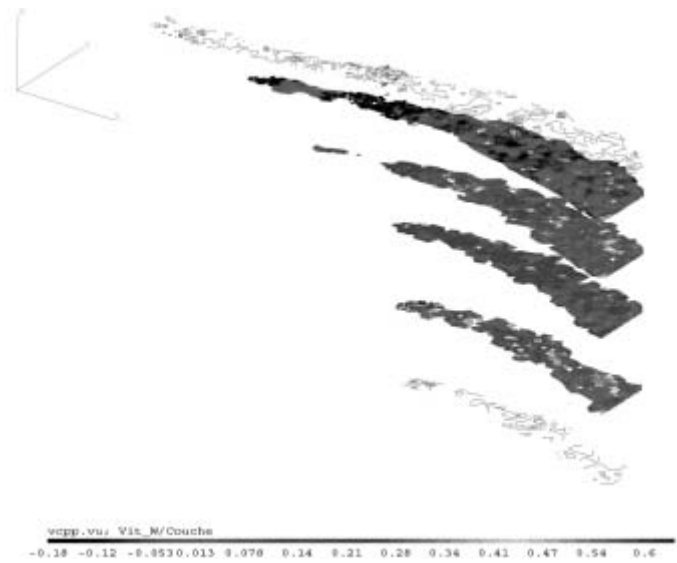


Fig. 19 Vertical velocity field ($\text{cm}\cdot\text{s}^{-1}$)

(see also ref. [7] and [17]). Despite these considerations, the present simulation deals only with the first expression for the water elevation, for which the numbers of elements and nodes for the surface layer are 3000 and 1652 respectively. Physical constants and parameters are listed below. A discharge of $11\,000\text{ m}^3\cdot\text{s}^{-1}$ of fresh water is specified on the upstream boundary of Ile d'Orléans balanced by a ratio of 30% vs and 70% on the north and south side of Ile d'Orléans respectively. Also $1300\text{ m}^3\cdot\text{s}^{-1}$ of water enters in the estuary at Tadoussac from the discharging of the Saguenay river. The steady-state flow is reached after three tidal cycles of approximately 37 hours.

Variable	Physical Constants	Values
ρ_a	Density of air	$1.3\text{ kg}\cdot\text{m}^{-3}$
ρ	Density of water	$1.010 \times 10^3\text{ kg}\cdot\text{m}^{-3}$
C_D	Wind drag coefficient	1.5×10^{-4} to 2.5×10^{-6}
N	Manning coefficient	$0.018\text{ s}\cdot\text{m}^{-1/3}$
ν	Horizontal eddy viscosity coefficient	$0.02\text{ m}^2\cdot\text{s}^{-1}$
f_{int}	Inter-layer friction coefficient	0.001
f_{ric}	Vertical eddy viscosity coefficient	10 m^2
Δt	Time step	
		$CFL.\text{max} \left(\frac{\min(V_R, V_L)}{S \left(u + c + 2\nu \frac{S}{V_s} \right)} \right)$
CFL	Stability criterion (courant number)	0.8
f_c	Coriolis parameter ($f_c = 2\omega \sin \iota$)	$\omega = 0.00008\text{ rad}\cdot\text{s}^{-1}$ and $\psi = 48.5^\circ\text{N}$
W_x	Longitudinal wind speed	$15\text{ m}\cdot\text{s}^{-1}$
W_y	Transversal wind speed	$3\text{ m}\cdot\text{s}^{-1}$

The next table presents the parameters used on the open boundary near Pointe-des-Monts for the M_2 constituent.

Constituent	Amplitude (m)	Period (h)	Phase delay (rad)
M_2	0.2	12.42	0.07
S_2	--	12.00	--
K_1	--	23.93	--
O_1	--	25.82	--

5.4 Conclusion

A complete model for solving three-dimensional environmental flows is given by the full Navier-Stokes equations. In this case, no attention needs to be paid to length scales between the vertical and the horizontal directions. Naturally, from the computer effort

point of view, this approach is more demanding than in 2-D or 3-D shallow water equations.

Although the full approach is more mature, if the nature of a class of problems exhibits a predominantly horizontal flow behavior, the SW model becomes a viable alternative from the numerical point of view; in particular, because there is no need to handle the divergence-free constraint, which implies a stiff problem to be solved. Also, the SW model, with a different type of equations (hyperbolic), is less demanding from the meshing point of view than the Navier-Stokes equations.

Staying with this line of thinking, in this paper a multi-layer finite-volume approach (*3-D SWE*) has been presented to solve free surface flows. With this approach, hydrodynamic basins can now take into account the complex and varying bathymetry by remeshing along the vertical 'wet' elements present on each layer. Validations on classical test cases have been demonstrated and, within the limits of the model, the approach has been applied to an actual configuration on the St. Lawrence estuary. As a future development of this work, it would be necessary to consider the variation in density of the different layers with an additional interpolation of the water elevation imposed on the open ocean boundary. Finally, it is noted that the water height variation is considered in physical units rather than a normalized quantity as given by the σ formulation introduced in ref. [19]. This approach provides an alternative which can be investigated in further studies to introduce moving and deforming layers.

Acknowledgements

The authors gratefully acknowledge the financial support of the NSERC (Natural Sciences and Engineering Research Council) and the Fondation de l'Université du Québec à Rimouski for this research. We would also like to thank the Center for Research on Computation and its Applications (CERCA) for their technical and logistic support.

References

- [1] FENNEMA, R.J. and CHAUDRY, M.H. 1986. Explicit numerical schemes for unsteady free-surface flows with shocks. *Water Resources Research*, 22: 1923-1930.
- [2] GARCIA, R. and KAHAWITA, R. 1986. Numerical solution of the St-Venant equations with the Mac-Cormack finite difference scheme. *International Journal for Numerical Methods in Fluids*, 6: 259-274.
- [3] JIMENEZ, O.F. and CHAUDRY, M.H. 1988. Computation of supercritical free-surface flows. *Journal of Hydraulic Engineering*, 114: 377-393.
- [4] KATOPODES, N.D. 1984. Two-dimensional surges and shocks in open channels. *Journal of Hydraulic Engineering*, 110: 794-812.
- [5] DHATT, G., SOULAMANI, A., OUELLET, Y. and FORTIN, M. 1986. Development of New Triangular Elements for Free Surface Flows. *International Journal for Numerical Methods in Fluids*, 6: pp. 895-911.
- [6] ZHANG, H. and REGGIO, M. 1995. A finite-volume solver for the shallow water equations in varying bed environments. *International Journal for Computational Fluid Dynamics*, 3: 233-250.
- [7] KODAMA, K., WANG, S.S.Y. and KAWAHARA, M. 1996. Model Verification on 3-D Tidal Current Analysis in Tokyo Bay. *International Journal for Numerical Methods in fluids*, 22: 43-66.
- [8] HESS, A. 1996. Modélisation numérique tridimensionnelle des écoulements à surface libre appliquée à des environnements de bathymétrie quelconque. Mémoire de Maîtrise ès Sciences Appliquées, Département de génie mécanique, École Polytechnique de Montréal, Montréal, P.Q, Canada.
- [9] ROE, P.L. 1981. Approximate Riemann Solvers, Parameter Vectors, and Difference Schemes. *Journal of Computational Physics*, 43: 357-372.
- [10] MATSOUKIS, P.F.C. 1992. The application of the method of characteristics for the simulation of nearly horizontal flow in two and three spatial dimensions. *International Journal for Numerical Methods in Fluids*, 14: 379-401.
- [11] TORO, C. 1992. Modélisation diagnostique de la circulation tridimensionnelle induite par la densité dans le golfe du Saint-Laurent. Thèse de Ph.D., Université du Québec à Rimouski, Rimouski, PQ, Canada.
- [12] ROE, P.L. 1986. Characteristic-Based Schemes for the Euler Equations. *Ann. Rev. Fluid Mech.*, 18: 337-365.
- [13] GLAISTER, P. 1988. A shock capturing scheme for body-fitted meshes. *International Journal for Numerical Methods in Fluids*, 8: 1095-1105.
- [14] GLAISTER, P. 1987. Difference scheme for shallow water equations. Technical Report, Dept. of Mathematics, University of Reading, Reading, U.K.
- [15] LYNCH, D.R. and GRAY, W.G. 1978. Analytic Solution for Computer Flow Model Testing. *Journal of the Hydraulics Division, ASCE*, 104: 1409-1428.
- [16] KOUTITAS, C. and O'CONNOR, B. 1980. Modeling three-dimensional wind-induced flows. *Journal of the Hydraulics Division, ASCE*, 107: 1843-1865.
- [17] CHASSÉ, E. J. 1994. Modélisation Numérique tridimensionnelle de la Circulation dans l'Estuaire du Saint-Laurent. Thèse de Doctorat, Département d'Océanographie de l'Université du Québec à Rimouski, Rimouski, PQ, Canada.
- [18] PHILLIPS, N.A. 1957. A coordinate system having special advantages for numerical forecasting. *J. Meteorol.*, 14: 184-185.
- [19] MELLOR, G.J. and BLUMBERG, A.F. 1985. Modeling vertical and horizontal diffusivities with the sigma coordinate system. *J. Phys. Oceanogr.* 113: 1379-1383.